THE PENNSYLVANIA STATE UNIVERSITY
SCHREYER HONORS COLLEGE

DEPARTMENT OF MATHEMATICS

SYMPLECTIC BILLIARDS

RAYMOND FRIEND
SPRING 2019

A thesis
submitted in partial fulfillment
of the requirements
for baccalaureate degrees
in Mathematics and Physics
with honors in Area of Mathematics

Reviewed and approved* by the following:

Sergei Tabachnikov
Professor of Mathematics
Thesis Supervisor

Richard Robinett
Professor of Physics
Honors Adviser

*Signatures are on file in the Schreyer Honors College.

Abstract

This document introduces a new planar billiards, first coined *symplectic billiards* in [1]. Symplectic billiards, when applied to polygonal boundaries, offers complicated behaviors with respect to periodicity. Various polygons are considered here, with progress made specifically in describing the behaviors in the affine space of quadrilaterals.

Table of Contents

List of Figures

Acknowledgements

I would like to thank my Thesis Supervisor: Dr. Serge Tabachnikov, for providing me support and impetus for this project. His passion for describing beautiful geometry has fully inspired this work. The entirety of the Penn State Mathematics Department has provided me an incredible environment in which to grow in mathematics.

Another thanks belongs to my Honors Advisor: Dr. Richard Robinett, for providing a new perspective on the future of symplectic billiards and for offering his full self in all of his students' pursuits.

I would finally like to acknowledge the unwavering support of my friends and family, especially my family in Penn State Club Cross Country. Their combined humility, strength, grace, and compassion have allowed me to maximize my potential as a student, athlete, leader, and friend.

Chapter 1

Introduction to Symplectic Billiards

1.1 Billiards as a Dynamical System

A billiard is a dynamical system that can be interpreted as the motion of a particle within or around a domain with a boundary. The particle follows an *orbit*, throughout which it is sent through either a finite or an infinite number of positions. Every billiard follows a particular rule for assigning the next location in a particle's orbit, and it is the differences in these rules and boundaries that explain the vast differences in behaviors between billiards.

The prototypical billiard example: the Birkhoff billiard, has been studied extensively. Its rule is identical to that of usual optics; a particle traveling from point x reflects elastically off of a boundary at point y so that the tangential component of its velocity is preserved while the perpendicular component alternates in sign, eventually finding the boundary again at point z. This is what physicists refer to when they say "the angle of incidence equals the angle of reflection." An example of Birkhoff billiards is displayed in Figure 1.1.
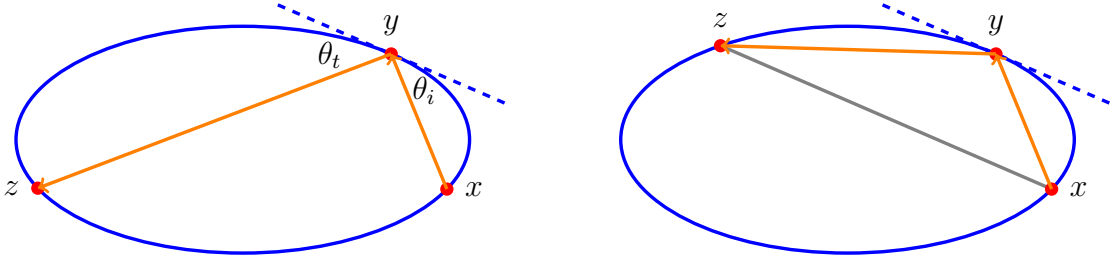

Figure 1.1: Left, the Birkhoff billiard, where $\theta_i = \theta_t$ implies the segment xy reflects to the segment yz. Right, the Symplectic billiard, where xz is parallel to the tangent line of the curve at point y implies xy reflects to yz.

One way to interpret the Birkhoff billiard is via its variational formulation: for fixed points x and z, the quantity $|xy| + |yz|$ is extremal for y along the boundary of the curve for precisely the y reflecting x to z in the billiard process [1]. Having a formula like this suggests that other variational formulations could produce different geometric rules for billiards. In fact, let's alter our billiards rule so that for fixed x and z, the point y is such that the *area* of the triangle xyz is extremal. This rule defines (and provides the namesake for) *symplectic billiards*. Geometrically, we can understand this rule to be as follows: a particle traveling from boundary points x to y will reflect towards point z if the line xz is parallel to the tangent line of the curve at point y.

Moving forward, we will agree that by *billiard*, we are referring to the symplectic billiard. If the boundary of the billiard curve is γ, an initial condition will consist of the pair (x_0, u_0), with x_0 a point along γ describing the initial position of the particle and u_0 a vector in $\mathbb{R}^2$ describing its initial velocity. The trajectory of an initial condition will be notated by

$$\text{Trajectory}_\gamma (x_0, u_0) = \{(x_0, u_0), (x_1, u_1), (x_2, u_2), ...\} \subset \gamma \times \mathbb{R}^2.$$

Alternatively, an initial condition can be given by $(x_0, x_1) \in \gamma \times \gamma$, where $\{x_0 + tu_0 : t \in \mathbb{R}\} \cap \gamma = \{x_0, x_1\}$. The orbit of an initial condition will be denoted

$$\text{Oribt}_\gamma (x_0, x_1) = \{x_0, x_1, x_2, ...\}.$$

Sometimes the subscript γ will be dropped whenever a particular γ is implicitly obvious.

1.2 Symplectic Billiards

We will more formally define the symplectic billiard. We will be considering smooth, strictly convex, closed, positively oriented curves, denoted by γ. By convexity, for each $x \in \gamma$ there exists a unique $x^* \in \gamma$ such that

$$T_x\gamma = T_{x^*}\gamma \subset \mathbb{R}^2.$$

The operation $*$ is obviously an involution. If η is the operator taking points on γ to their normal vector to γ, then we have the equivalence:

$$T_x\gamma = T_y\gamma \text{ if and only if } \omega\left(\eta_x, \eta_y\right) = 0, \tag{1.1}$$

where ω is the area form, defined on the tangent space of γ. The comparison $x < y < z$ is well-defined as γ is oriented, so we can define

$$\mathcal{P}_\gamma := \{(x,y) \in \gamma \times \gamma : x < y < x^*\} = \{(x,y) : y^* < x < y\} = \{(x,y) : \omega\left(\eta_x, \eta_y\right) > 0\},$$

which we call the open, positive part of phase space to the symplectic billiard map Φ_γ. This map is defined below.

Definition 1.2.1. *Let γ be a smooth, strictly convex, closed, positively oriented curve. For $(x,y) \in \mathcal{P}$, define the symplectic billiard map $\Phi_\gamma : \mathcal{P} \to \mathcal{P}$, $\Phi_\gamma(x,y) = (y,z)$, where z is the unique point in γ such that $z - x \in T_y\gamma$.*

We are obligated to show that Φ (dropping the subscript for ease of notation) is well-defined. Note first that $(x,y) \in \mathcal{P}$ implies that their tangent spaces are transversal. And γ being convex implies that

$$(x + T_y\gamma) \cap \gamma = \{x, z\}.$$

But z is distinct from x. Otherwise, $T_y\gamma = T_z\gamma = T_x\gamma$, and so by Equation (1.1), $\omega\left(\eta_x, \eta_y\right) = 0$, a contradiction to $(x,y) \in \mathcal{P}$. Thus, we at least have that $z - x$ is an element of $T_y\gamma$. We still should explain why $(y,z) \in \mathcal{P}$. There are two main observations: first, that if x is sufficiently close to y, then z is close to y as well, meaning $\omega\left(\eta_x, \eta_y\right) > 0$ implies $\omega\left(\eta_y, \eta_z\right) > 0$ in this case; and second, ω is continuous. So if $x < y < x^*$ yet $\omega\left(\eta_y, \eta_z\right) \leq 0$, then as we move y closer to x, the continuity of ω allows us to find a y such that $\omega\left(\eta_y, \eta_z\right) = 0$. But then again by Equation (1.1), we have $T_y\gamma = T_z\gamma$, so $x = y$, a contradiction.

Following the discussion of [1], we know have that Φ continuously extends to the entire phase space, including

$$\Phi\left(x,x\right) = \lim_{y \to x} \Phi(x,y) = (x,x),$$
$$\Phi\left(x,x^*\right) = \lim_{y \to x^*} \Phi(x,y) = (x^*,x).$$

Chapter 2

Introduction to Polygonal Symplectic Billiards

2.1 Affine Polygons

A competing name for the symplectic billiard is the *affine billiard*, because this dynamical system commutes with all affine transformations of the plane. Reconsider the defining rule of affine billiards: nowhere does absolute scale or position explicitly matter in constructing an orbit, only the notion of parallel lines.

Lemma 2.1.1. *Any affine transformation f of the billiard table commutes with the symplectic billiard map in the following way: if $x, y \in \gamma$ are such that $\Phi(x, y) = (y, z)$, then*

$$\Phi(f(x), f(y)) = (f(y), f(z)).$$

Proof. Any affine transformation f may be written as the composition of a linear map g and a translation h, i.e. $f = h \circ g$. Therefore, it is sufficient to show $h \circ \Phi = \Phi \circ h$ and $g \circ \Phi = \Phi \circ g$, since

$$\Phi \circ f = \Phi \circ (h \circ g) = h \circ \Phi \circ g = h \circ g \circ \Phi = f \circ \Phi.$$

Let $h(x) = x + \alpha$ for fixed $\alpha \in \mathbb{R}^2$. Suppose that $x, y, z \in \gamma$ so that $\Phi(x, y) = (y, z)$, meaning z is the unique point in γ so that $z - x \in T_y\gamma$. Notice that since $x - z \in T_y\gamma$, then it must be that

$$g(z) - g(x) = g(z - x) \in T_{g(y)}g(\gamma).$$

So $\Phi(g(x), g(y)) = (g(y), g(z))$. Next, we see that

$$h(z) - h(x) = (z + \alpha) - (x + \alpha) = z - x \in T_y\gamma = T_{y+\alpha}(\gamma + \alpha) = T_{h(y)}h(\gamma).$$

Therefore, $\Phi(h(x), h(y)) = (h(y), h(z))$. We are done. $\qquad\square$

Now, we must remark that having γ be a polygon does not satisfy the *strict*-convexity nor the smoothness condition of Definition 1.2.1. However, we can describe the scenarios in which the symplectic billiard map is undefined on a closed, convex, positively oriented polygon γ. The first case is that Φ is not well-defined if x or y is a vertex of the polygon. Second, the map is not defined for chord xy if x and y lie on parallel edges of the polygon. A minor but useful result helps to ease our concerns about such cases:

Lemma 2.1.2. *For convex polygon γ, so long as $\Phi(x, y) = (y, z)$ is well-defined, and if x and y do not lie on parallel edges of γ, then y and z will not lie on parallel edges of γ.*

Proof. Suppose otherwise. By definition,

$$z - x \in T_y\gamma = T_z\gamma \implies x \in T_z\gamma.$$

Thus, $T_x\gamma = T_z\gamma = T_y\gamma$, a contradiction. Moreover, $\qquad\square$

We note that even if $\Phi(x, y) = (y, z)$ is well-defined, it may be that $\Phi(y, z)$ is not. This is only possible if z is a vertex of γ. We can characterize the set of $(x, y) \in \gamma \times \gamma$ such that, if $\Phi(x, y) = (y, z)$ exists, z is vertex. Fix edge k, and let z be a vertex of γ. Take y an interior point of edge k. If

$$\#\left[((z + T_y\gamma) \cap \gamma) \setminus \{z\}\right] = 1,$$

then take x as its only element. This guarantees that (x, y) has its first image as (y, z) for z a vertex of γ. Any preimages of (x, y) will eventually have an image terminating at a vertex. However, and obviously, there are finitely many vertices of γ, and only one x per edge for fixed vertex; so the set of all $(x, y) \in \gamma \times \gamma$ that eventually terminate in a vertex is of Lebesgue measure zero.

We conclude this section by describing the phase space of Φ for a convex polygonal γ. The phase space is a subset of the torus $\gamma \times \gamma$, which decomposes into rectangles representing the product of pairs of edges on γ. If two edges are parallel on γ, then their respective rectangle does not lie in the phase space. There may also exist horizontal or vertical lines within these rectangles where Φ is undefined because they eventually terminate in a vertex.

2.2 Regular Affine Polygons

Our analysis of regular polygons shall make use of their symmetries. First, we agree to index the sides of the n-gon cyclically in the positive direction, from 0 to $n - 1$. Label the vertices in the natural way, starting with v_0 and v_1 on edge 0, and so on. We may assume without loss of generality that the initial segment runs from edge 0 to edge k, with $1 \le k \le \lfloor (n-1)/2 \rfloor$. The quantity k is traditionally called the *rotation number* of the orbit [1]. Albers and Tabachnikov produce the following result in [1].

Theorem 2.2.1. *(i) The rotation number of an orbit is constant across each step in the orbit, sending a point on edge i to the edge labeled $i + k \mod n$.*

(ii) Define

$$g(n, k) := \frac{n}{\gcd(n, 2k)}.$$

Then, generically,

(a) Every orbit of rotation number k with $g(n, k)$ even is periodic with period $2g(n, k)$.

(b) Every orbit of rotation number k with $g(n, k)$ odd is periodic with period $4g(n, k)$.

Proof. (i) Let us enumerate the vertices of the polygon $0, ..., n - 1$, following the same orientation as γ, with edge 0 labelled by $\overline{0\,1}$, etc. Let x_0 and x_1 denote the first and second point in the orbit of x_0, respectively. Point x_0 lies on edge 0 and x_1 lies on edge k. A fact about regular polygons is that for $1 \le k < \lfloor (n-1)/2 \rfloor$, the quadrilateral $[0, 1, 2k, (2k+1)]$ is a trapezoid, with $\overline{1\,2k}$ and $\overline{0\,(2k+1)}$ both parallel to the k-th side of γ. Therefore, there exists some x_2 on edge $2k$ such that

$$x_2 - x_0 \in T_{x_1}\gamma.$$

This establishes that every point on edge k maps to the same edge $k + k = 2k$. By dihedral symmetry, this implies every point on edge i maps to the same edge $i + k$. Note, that if n is odd and $k = (n-1)/2$, then the quadrilateral is degenerately a triangle $[0, 1, 2k]$. Still, the edge $\overline{1\,2k}$ is parallel to edge k, and the line parallel to these and passing through edge 0 only intersects γ at 0. Therefore, edge k maps onto edge $2k$, and our argument still applies.

(ii) Take an orbit $x_0, x_1, ...,$ and assume without any loss of generality that x_0 lies on edge labeled 0, and x_1 on edge k. By (i), x_i lies on edge $i \cdot k$. We notice that the segments connecting x_0

with x_2, x_2 with x_4, etc. are each parallel to an edge of γ, and similarly for x_1, x_3, x_5, etc. We call these two polygonal lines even and odd, respectively.

We claim that the symmetry of a regular polygon implies the even and odd polygonal lines are actually Birkhoff billiard orbits. If ℓ_i denotes the edge of γ on which x_i lies, with endpoints v_{ℓ_i} and v_{ℓ_i+1}, then by the same argument as (i), the quadrilaterals

$$[x_0, v_{\ell_1}, v_{\ell_1+1}, x_2] \qquad \text{and} \qquad [x_2, v_{\ell_3}, v_{\ell_3+1}, x_4]$$

are both trapezoids, since, for example, $x_2 - x_0 \in T_{x_1}\gamma$. We notice that, by dihedral symmetry, x_0 and x_2 have complementary positions on their their respective edges. I.e. if s_i is such that

$$x_i = s_i \cdot v_{\ell_i+1} + (1 - s_i) \cdot v_{\ell_i},$$

then $s_2 = 1 - s_0$. Thus, $s_4 = 1 - s_2 = s_0$. Because x_4 lies on side $4k$, it must be that the two trapezoids are congruent, and so the even polygonal line is a Birkhoff orbit. The same applies to the odd orbit.

Now let us restrict our attention to the particular initial conditions: x_0 and x_1 as midpoints of their respective edges. These conditions imply that x_i is the midpoint of edge $i \cdot k$ for each i. The even Birkhoff orbit connects midpoint of edge 0 to that of edge $2k$, so it has period

$$\frac{n}{\gcd(n, 2k)} = g(n, k).$$

For any other choice of x_0, the even trajectory will be a parallel trajectory to the midpoint trajectory, but will either have period $g(n, k)$ if $g(n, k)$ is even, or $2g(n, k)$ if $g(n, k)$ is odd. This follows from the previous observation that x_{2m} and $x_{2(m+1)}$ take on complementary positions. Obviously, then, the even orbit only depends on choice of x_0, while the odd orbit only depends on the choice of x_1. So the even and odd orbits are generally distinct. In general, we see that the period of the (symplectic) orbit $x_0, x_1, \ldots$ is $2g(n, k)$ if $g(n, k)$ is even, and $4g(n, k)$ if $g(n, k)$ is odd.

$\square$

The above argument is notable for two reasons. First, it identifies the usual (Birkhoff) billiard lurking within the symplectic billiard in a regular affine polygon, an unexpected connection between the two. Second, it establishes that while there may exist unusual orbits within a regular polygon that do not satisfy the theorem, those orbits comprise a set of measure zero in the phase space. Nevertheless, these orbits will all be periodic, perhaps with smaller period due to an overlap between the even and odd orbits. For example, every triangle has a 3-periodic orbit connecting the midpoints of its edges.
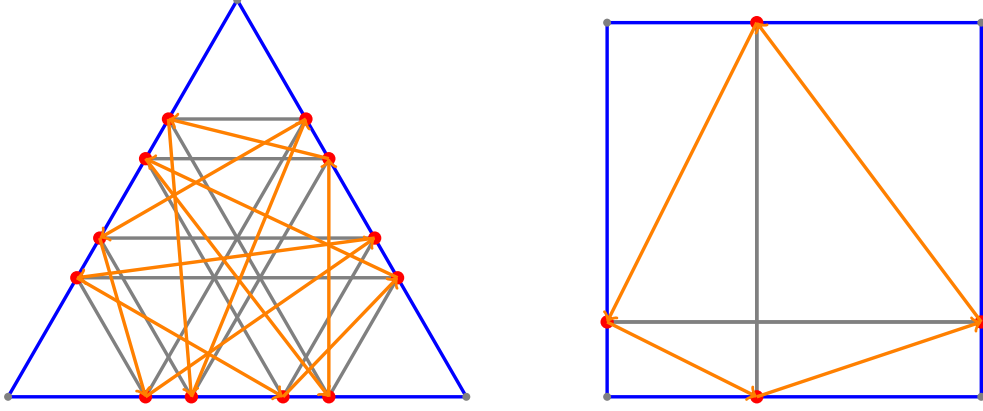
Figure 2.1: Left, a 12-periodic symplectic orbit in a triangle of $k = 1$. Right, a 4-periodic symplectic orbit in a square of $k = 1$. Gray orbits are Birkhoff.
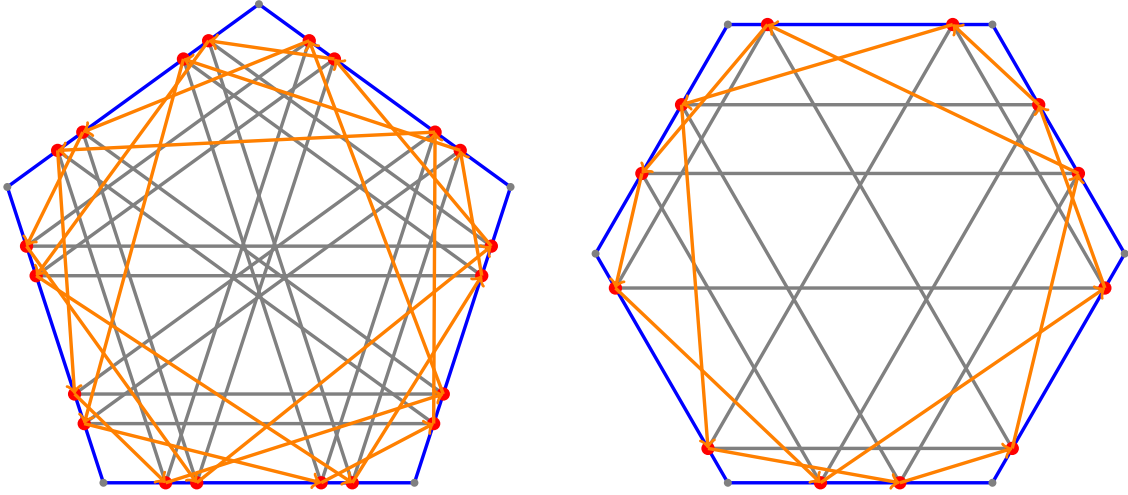

Figure 2.2: Left, a 20-periodic symplectic orbit in a regular pentagon of $k = 1$. Right, a 12-periodic symplectic orbit in a regular hexagon of $k = 1$. Gray orbits are Birkhoff.

2.3 Periodicity within Affine Polygons

Let us denote the n-periodic, symplectic, polygonal orbit by $(x_0, x_1, ..., x_{n-1})$. Call ℓ_i the line parallel to $x_{i-1}x_{i+1}$ through x_i.

We may consider a nearby orbit $(\overline{x}_0, \overline{x}_1, ...)$ made from $\overline{x}_0 \in \ell_0$ and $\overline{x}_1 \in \ell_1$, and immediately decouple its even and odd orbits. In particular, the even orbit is generated by projecting $\overline{x}_0$ along ℓ_1 to ℓ_2, then along ℓ_3 to ℓ_4, etc.; and similar for $\overline{x}_1$. We denote by π_i the projection along ℓ_i of ℓ_{i-1} to ℓ_{i+1}.

Call α_i the angle between ℓ_i and ℓ_{i+1}. And define dl_i as the length element on ℓ_i. Then we describe how the affine projection π_i distorts length by the factor

$$\frac{d\ell_{i+1}}{d\ell_{i-1}} = \frac{\sin \alpha_{i-1}}{\sin \alpha_i}.$$

Theorem 2.3.1. *For n odd, any n-periodic symplectic orbit has an open neighborhood in phase space for which each neighbor is $4n$-periodic.*

Proof. The first time that a neighboring $\overline{x}_0$ returns to ℓ_0 is after n projections, precisely

$$\pi_{\text{even}} = \pi_{n-1} \circ \cdots \circ \pi_2 \circ \pi_0 \circ \pi_{n-2} \circ \cdots \circ \pi_1.$$

Their composition is affine, reverses orientation, and is an isometry since the overall distortion factor is

$$\prod_{i=0}^{n-1} \frac{d\ell_{i+1}}{d\ell_{i-1}} = \prod_{i=0}^{n-1} \frac{\sin \alpha_{i-1}}{\sin \alpha_i} = 1,$$

where $\ell_{-1} = \ell_{n-1}$. Thus, $\pi_{\text{even}}^2 = \text{id}$. Applying a similar argument for $\overline{x}_1$, we have that the even and odd orbits each consist of $2n$ points, so the orbit of $(\overline{x}_0, \overline{x}_1)$ is $4n$-periodic. Because $\pi_{\text{even}}^2 = \pi_{\text{odd}} = \text{id}$, there exists an open neighborhood so that all neighbors of (x_0, x_1) in phase space have the same $4n$-periodicity. $\qquad\square$

This result implies that no polygonal γ may have a sequence of odd-periodic orbits that are arbitrarily close in phase-space, even if they are of the same period. It is natural to ask what we can say about even-periodic orbits now.

Theorem 2.3.2. *If $n \geq 6$ is even, then an n-periodic orbit on a generic polygon will be isolated, yet stable under any small perturbations of the polygon.*

Proof. The first time that a neighboring $\overline{x}_0$ returns to ℓ_0 is after $\frac{n}{2}$ projections, precisely

$$\pi_{\text{even}} = \pi_{n-1} \circ \cdots \circ \pi_3 \circ \pi_1.$$

The corresponding set of projections for $\overline{x}_1$ is

$$\pi_{\text{odd}} = \pi_0 \circ \cdots \circ \pi_4 \circ \pi_2.$$

If either of these affine maps' distortion factors

$$\prod_{i \text{ odd mod } n} \frac{\sin \alpha_{i-1}}{\sin \alpha_i}, \qquad \prod_{i \text{ even mod } n} \frac{\sin \alpha_{i-1}}{\sin \alpha_i}$$

is different from 1 (a generic property), then the n-periodic point (x_0, x_1) is isolated, since x_0 is isolated for the first quantity different than 1, and x_1 is isolated for the second quantity different than 1. It is a generic property that points with both distortion factors different than 1 (i.e. hyperbolic fixed points) do not vanish under small perturbations of the map, and hence the polygon. $\qquad\square$

Chapter 3

Convex Affine Quadrilaterals

3.1 Space of Convex Affine Quadrilaterals

A corollary of Theorem 2.2.1 is that all symplectic orbits on a triangle are 12-periodic, since every triangle is affine-equivalent [2] (in particular, to an equilateral triangle) and Φ commutes with any affine transformation according to Lemma 2.1.1.

It is natural to next consider the behavior of symplectic billiards on quadrilaterals. We already have a strong result on the subclass of quadrilaterals affine-equivalent to a square. We first note that the affine space of quadrilaterals on the plane is two-dimensional. So we can imagine representatives from each affine-equivalence class by fixing two adjacent edges of a square, each of length 1, to the origin and oriented on the positive axes, with a final vertex free to roam part of the plane. Taking into account reflections, we can reduce the affine space of quadrilaterals to the region between the angles of 0 and $\frac{\pi}{4}$. Moreover, because we require convexity, it must be that the fourth point lies above $y = 1 - x$. This is not the full reduction of the plane into a one-to-one representation of the affine space of quadrilaterals. Such a space is more complicated: for example, given P, it is possible to find a family of affine maps mapping the original P-quadrilateral to an AP-quadrilateral whose edges adjacent to AP are of unit length and perpendicular, AP lies in the region, and the AP-quadrilateral is congruent to the P-quadrilateral. More analysis can be taken to refine this space.

Keeping in mind the previous point, the following Figure 3.1 illustrates a redundant space of affine, convex quadrilaterals, which we call $\mathcal{Q}$.
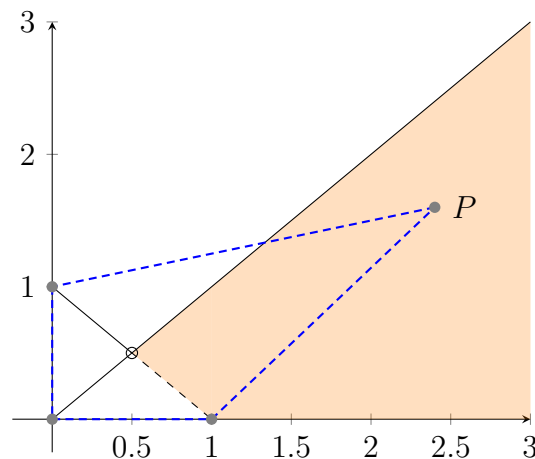

Figure 3.1: The affine space of convex quadrilaterals $\mathcal{Q}$. P is the only free point. The point $P = (1, 1)$ corresponds to the class of affine squares. Either of the lines $x = 1$ or $y = 1$ represent all affine trapezoids. And the line $y = x$ represents all kites.

3.2 Affine Trapezoids

Another positive result coming from [1] regards trapezoids. The authors first ask that trapezoid $ABCD$ is adjusted by an affine transformation to be isosceles. Next, assume that the lower horizontal side AB of trapezoid $ABCD$ is longer than upper horizontal CD. They define the modulus

of a $ABCD$ as follows:
$$\left\lfloor \frac{|AB|}{|AB| - |CD|} \right\rfloor \in \mathbb{N}.$$
They describe a trapezoid as generic if $|AB| / (|AB| - |CD|)$ is not an integer.

Theorem 3.2.1. *Every orbit on a generic trapezoid of modulus n is periodic, with period either $16n - 4$, $16n + 4$, or $16n + 12$.*

Proof. First, we shall define a map F along the boundary of the trapezoid. If X is an interior point of a side of the trapezoid, notice that there pass two lines through X that are each parallel to a side of the trapezoid. We may arbitrarily choose one of them, and follow that ray until it intersects with the boundary again at point Y. Again, if Y is an interior point, then there pass two lines parallel to sides of the trapezoid, one of which was the originally chosen segment XY. We choose the remaining line and find where it intersects the boundary again at Z. Continuing this process, we have described the map $F : X \mapsto Y \mapsto Z \mapsto \cdots$.

Notice that every orbit of F within a trapezoid visits every edge, so we can limit our starting conditions to $X \in BC$, and move horizontally left towards $Y \in AD$. Then it must be that $Z \in AB$. Once here, the behavior of F guarantees a certain number of oscillations between the top and bottom edges. Eventually, some point on AB heads in the direction parallel to AD and intersects BC. We let T be the return map describing the first iterate of X under F on BC.

The number of bouncing moves between AB and CD under T depends on the position of X along BC. In fact, there exists interior point E of BC so that $T(E) = C$ and if $X \in EC$, then the number of bouncing moves is $2(n - 1)$, while if $X \in BE$, it equals $2n$. To find E, simply backtrack from C via a line parallel to AD and continue by applying F until intersecting BC.
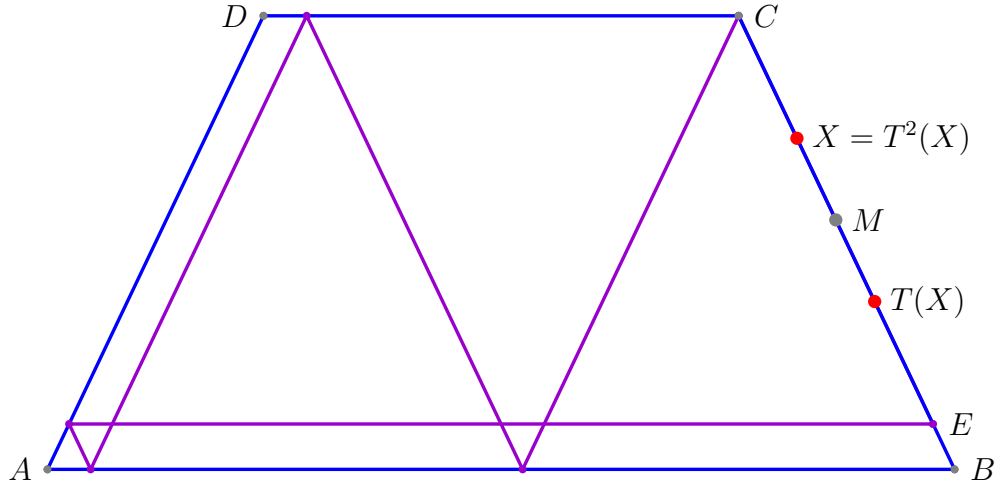

Figure 3.2: To find the break point E of the trapezoid $ABCD$, retreat from C parallel to AD, then retreat again parallel to BC, and continue until reaching AD, where you retreat parallel to AB, finding E along BC. In the illustration, $n = 2$. If M is the midpoint of segment EC, then T is the reflection in M for X on EC.

F must act an odd number of times in order to reach BC again, and so T reverses orientation. Moreover, we can see that T is a local isometry, as moves between the top and bottom sides have

distortion factor 1, and the two moves AD to AB and AB to BC distort with reciprocal factors. Thus, T must be a reflection in a point; a quick check shows that that point is either in the midpoint of BE or the midpoint of EC. This is enough to conclude that the period of X under T equals $4n + 2$ if $X \in EC$, and $4n + 6$ if $X \in BE$, since there are 3 points beyond the bouncing for each of the two cycles.

With this, we consider a symplectic billiard orbit $x_0, x_1, ...$ in the trapezoid. Breaking the orbit into its even and odd parts, whose segments between adjacent points are parallel to the edges of the trapezoid, we see that both the even and odd parts are finite and so the orbit is periodic. To calculate the period of the orbit, we must consider some cases.

We consider the orbits of x_0 and x_1 under F: either may be short or long (distinguished by whether they have length $4n + 2$ or $4n + 6$, respectively). Therefore, and aligned with the terminology of [1], we shall consider three cases: short-short, short-long, and long-long. Each will have different periods.
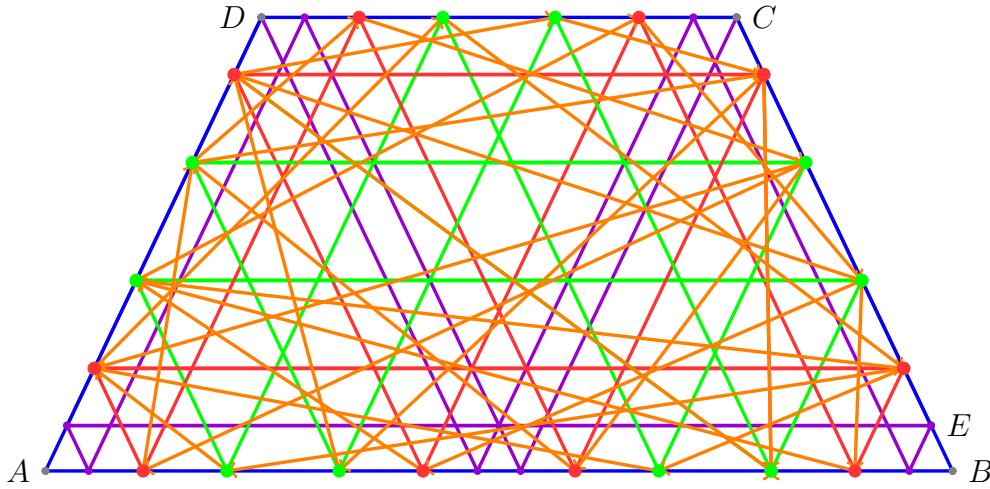

Figure 3.3: Example of a short-short orbit. The orbit is drawn in orange, even orbit in green, odd orbit in red, and break point lines in purple. This is a 28-periodic symplectic orbit in an isosceles trapezoid where $|AB| / (|AB| - |CD|) = 2.1$, so $n = 2$, and $28 = 16(2) - 4$.

In Figure 3.3, we notice that a short-short orbit in general appears very disorderly, even for $n = 2$. Yet, we can simplify our illustration by aligning the F-orbits of x_0 and x_1 and by beginning at M: the midpoint of EC and fixed point of T; and note that this simplification will reduce the number of points in the orbit to a quarter of the non-aligned case. The combined F-orbit of x_0 and x_1 has $2n + 1$ vertices, with one on M and one on the corresponding midpoint on DA, n on AB, and $n - 1$ on the above CD. Suppose these points are labeled as displayed in Figure 3.4.
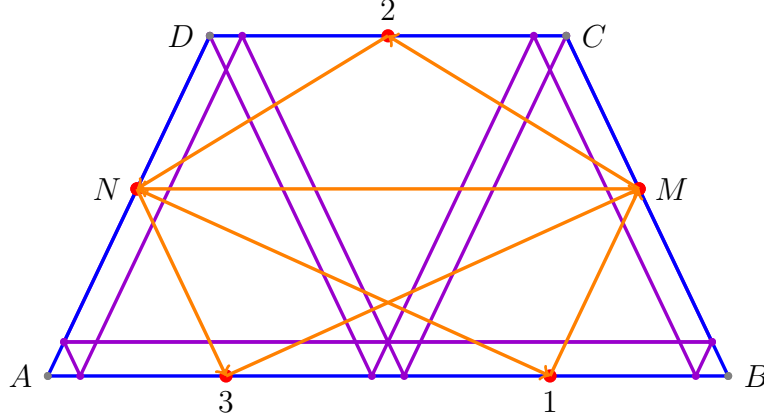
Figure 3.4: The simplified diagram for short-short.

We see that the symplectic billiard orbit is $4n - 1$ periodic with the following sequence of points:

$$(1, M, 2, N, 3, M, 4, ..., (2n - 1), M, N).$$

In Figure 3.4, this sequence is $(1, M, 2, N, 3, M, N)$. Now we consider the generic short-short orbit: it will have four times as many points, so a generic short-short period is $16n - 4$ periodic.

One can analyze the long-long case in an analogous manner, taking into account the four extra oscillations for the F-orbits of x_0 and x_1, which quadruple to 16 additional points along the orbit than the short-short case. So the long-long case corresponds to $16n + 12$ periodic symplectic orbits.

Finally, the short-long case is slightly more complicated. It may be summarized by a similar sequence of points after simplifying the shape by aligning the F-orbits and similar positioning about the midpoints of segments defined by the breaking points on each side-edge. It can be seen that the symbolic orbit may be written as

$$(N, I, M, II, N, III, M, ..., (2n - 1)I, M, P, 1, Q, 2, P, 3, Q, 4, ..., (2n + 1), Q).$$

This generally offers $8n + 2$ points. The orbit doubles in size for the generic case, and thereby shows short-long orbits have period $16n + 4$.

$\square$

3.3 General Convex Affine Quadrilaterals

The remainder of this paper shall focus on the unstudied cases of quadrilaterals that are not parallelograms or trapezoids. We notice immediately that for any orbit satisfying the generic conditions of Theorem 2.3.2 along a trapezoid, a small perturbation in the shape will not remove the periodic orbit (since the periodicity of orbits along a trapezoid are no smaller than 12). Moreover, for any orbit satisfying the generic conditions of Theorem 2.3.2 along a triangle, a small perturbation of the triangle into a quadrilateral will not remove the 12-periodic orbit. Analyzing the general quadrilateral, though, is not a simple task, as much of the symmetry present in squares and trapezoids is lost in the general case. The dihedral symmetry of a regular polygon, and our ability

to have F be a well-defined map with only one or two options at each point along a trapezoid, are specifically what we lose in the larger scope of $\mathcal{Q}$.

A natural way to break up our analysis of quadrilaterals will be as follows. Label the vertices of our quadrilaterals from $\mathcal{Q}$ by $0, 1, 2, 3$, where 0 lies on the origin, 1 at $(1, 0)$, 2 at P, and 3 at $(0, 1)$. The angles at vertices 1 and 3 are very relevant to the behavior of orbits along γ. In particular, we care whether these angles are acute (A) or obtuse (B). In the case both are acute, we label the resulting quadrilateral as coming from $AA \subset \mathcal{Q}$. Likewise, if the angle at 1 is obtuse and the angle at 3 is acute, we label this BA. And both obtuse corresponds to BB.
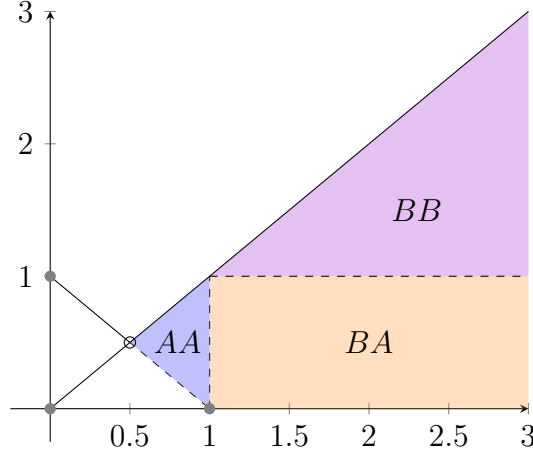

Figure 3.5: The affine space of convex quadrilaterals $\mathcal{Q}$ decomposed into its three subregions: AA, BA, and BB.

Any refinement of $\mathcal{Q}$ (as mentioned in the beginning of the section) would respect these three regions, meaning equivalence classes of points would be separated into these regions. The following result holds for a small class of orbits on AA and BA quadrilaterals (but we restrict ourselves to the case of BA for simplicity. The extension to AA is exactly the same but with an extra condition on the maximum value of the first coordinates).

Theorem 3.3.1. *Let us suppose γ is a quadrilateral from BA, whose fourth vertex is $P = (a, b)$, where $a + 2b < 2$. If α is defined as*

$$\alpha = \frac{a}{1 - b} - 1,$$

and t, s are such that

$$\frac{\alpha}{1 + \alpha} < t, s < \frac{1}{1 + \alpha},$$

then the orbit resulting from the initial conditions

$$x_0 = (0, t), \qquad x_1 = ((1 + \alpha)(1 - s), s)$$

will be 12-periodic.

Proof. We notice that $0 < \alpha < 1$ by construction. Define the triangle

$$\mathcal{T} = \{(0, 0), (1 + \alpha, 0), (0, 1)\}.$$

This triangle encompasses the bottom edge of the quadrilateral, but extends to the point $(1+\alpha, 0)$. It also encompasses the top edge, meeting point P and continuing to $(0, 1)$. Finally, the triangle shares its left edge with that of the quadrilateral.

Such t, s exist as specified in the statement of the theorem because $\alpha < 1$. What is really happening here is that the entirety of the orbit will lie on the parts of the edges $0, 2$ and 3 that are in common with $\mathcal{T}$. And because every orbit on a triangle is 12-periodic, the same will be true for this orbit. In order to see this behavior, one can explicitly calculate the 12 coordinates along the orbit: what will be important to check is that maximum of the first coordinate for each point does not exceed 1. Assuming the orbit stays within these parts, the coordinates of the full orbit are as follows:

$$
\begin{aligned}
x_0 &= (0, t), & x_1 &= ((1+\alpha)(1-s), s), & x_2 &= (t(1+\alpha), 0), \\
x_3 &= (0, s), & x_4 &= (t(1+\alpha), 1-t), & x_5 &= ((1+\alpha)s, 0), \\
x_6 &= (0, 1-t), & x_7 &= ((1+\alpha)s, 1-s), & x_8 &= ((1-t)(1+\alpha), 0), \\
x_9 &= (0, 1-s), & x_{10} &= ((1-t)(1+\alpha), t), & x_{11} &= ((1-s)(1+\alpha), 0).
\end{aligned}
$$

Notice that the maximum values of each coordinate include $t(1+\alpha)$, $s(1+\alpha)$, $(1-t)(1+\alpha)$, $(1-s)(1+\alpha)$. By our choice of t and s, all four of these quantities are strictly less than 1. Therefore, we have that this orbit is well-defined and is a consequence of the dynamics of the triangle $\mathcal{T}$. $\qquad\square$

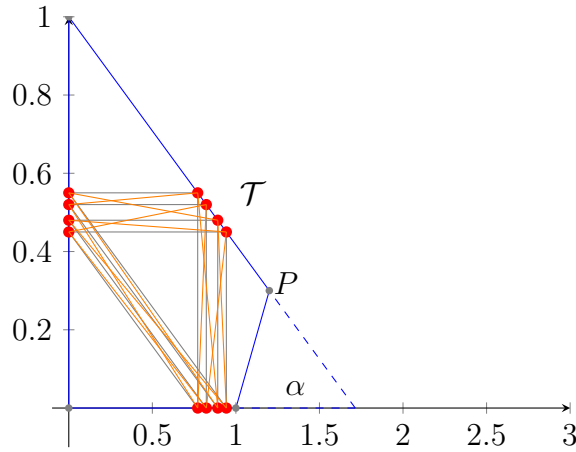Figure 3.6: The dynamics of the triangle $\mathcal{T}$ apply to this orbit on this quadrilateral because the orbit lies only on sides touching $\mathcal{T}$.

Moreover, it is true that any symplectic orbit strictly containing points along three edges will necessarily be 12-periodic. Below is an example of a quadrilateral beyond the statement of Theorem 3.3.1 with a 12-periodic orbit staying on three edges.
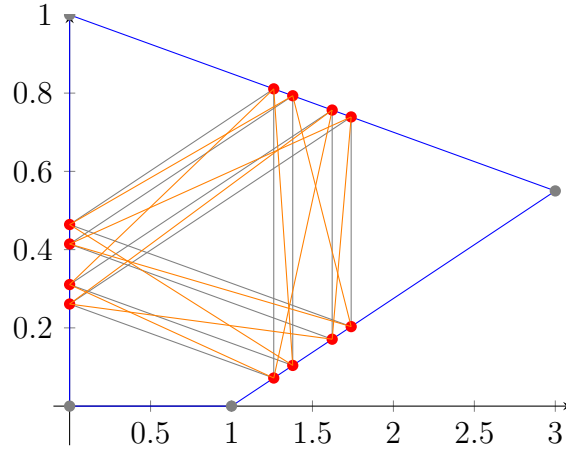
Figure 3.7: An orbit along this quadrilateral remains on the same three sides. Thus, we can imagine the orbit lying along a triangle, and hence is 12-periodic. The initial conditions for this image were $P = (3, 0.55)$, $t_0 = 1.2609$, and $\theta_0 = 17°$.

Similar analyses of certain quadrilaterals and their orbits are possible, but are likely not sufficient to describe the entire space of affine quadrilaterals $\mathcal{Q}$. Now we present the phase space of each type of quadrilateral, as well as those for a square and trapezoid for better comparison. We label each region of the phase spaces, on which Φ restricts to an affine map, with the corresponding edge to which an initial condition from this region would be sent. So, for a cell in column i and row j, filled in with k, we read this as x_1 on edge j sends x_0 from edge i to x_2 on edge k. Any splits in the cells represent that x_0 is either sent to one of these two edges (but there is a dividing E along edge i that separates these two possibilities). Moreover, we can provide a second table summarizing the 2-step process, i.e. the location of x_3 given x_0 and x_1.

3	2	1	0	0	(gray)
2	3	3	(gray)	1 | 0	
1	3 | 2	(gray)	0	0	
0	(gray)	3	3	2 | 1	
x_1/x_0	0	1	2	3	

3	1 | 0 | 0	2 | 1	2 | 1	(gray)
2	0	0	(gray)	0 | 3
1	0 | 3	(gray)	3	3
0	(gray)	2 | 1	2 | 1	3 | 3 | 2
x_1/x_0	0	1	2	3

Figure 3.8: The 1-step and 2-step phase spaces for quadrilaterals of acute-acute (AA) type.

x_1/x_0	0	1	2	3
3	2	2	1 | 0	▓
2	3	3	▓	1 | 0
1	2	▓	0 | 3	2
0	▓	3	3	2 | 1

x_1/x_0	0	1	2	3
3	1 | 0	1 | 0	2 | 2 | 1	▓
2	1 | 0	1 | 0	▓	0 | 3 | 3
1	3	▓	3 | 2	3
0	▓	2	2	3 | 2

Figure 3.9: The 1-step and 2-step phase spaces for quadrilaterals of obtuse-acute (BA) type.

x_1/x_0	0	1	2	3
3	2	2	1 | 0	▓
2	1	0 | 3	▓	1
1	2	▓	0 | 3	2
0	▓	3 | 2	1	1

x_1/x_0	0	1	2	3
3	1	1	2 | 1	▓
2	0 | 3	1 | 1 | 0	▓	0 | 3
1	0 | 3	▓	3 | 2 | 2	0 | 3
0	▓	2 | 1	2	2

Figure 3.10: The 1-step and 2-step phase spaces for quadrilaterals of obtuse-obtuse (BB) type.

x_1/x_0	0	1	2	3
3	1	0	▓	▓
2	1	0	▓	▓
1	▓	▓	3	2
0	▓	▓	3	2

x_1/x_0	0	1	2	3
3	2	2	▓	▓
2	3	3	▓	▓
1	▓	▓	0	0
0	▓	▓	1	1

Figure 3.11: The 1-step and 2-step phase spaces for squares (type $\perp\perp$).

3	2	2	1	0	
2		3			1
1	2		0	3	2
0		3			1
x_1/x_0	0	1	2		3

3	1	1	2	1		
2		1	0		0	3
1	3		3	2	3	
0		2			2	
x_1/x_0	0	1	2		3	

Figure 3.12: The 1-step and 2-step phase spaces for trapezoids of perp-obtuse ($\perp B$) type. These are equivalent to considering those of acute-perp type.

These tables provide a summary of the dynamics for the even and odd orbits as well. The simplicity of the charts for squares and trapezoids is just enough to make them predictable, but it is unlikely that the dynamics of general quadrilaterals will be totally explainable. It may very well be that this problem resembles another problem from billiards: that of finding periodic Birkhoff orbits within triangles. While these two problems may seem like natural questions to investigate, solving them may bring us no closer to understanding the dynamics. Moreover, the following section will show calculated results about quadrilaterals that suggest a variety of behaviors are possible. It may be possible to show that there exists some standard dynamical system lurking within the dynamics of the general quadrilaterals, the same way we found Birkhoff billiards occurring within regular polygons, or the particular codes in the case of the trapezoids, but it will likely depend on the defined types of quadrilaterals: AA, BA, and BB.

Chapter 4

Computational Approach

4.1 Computing a Symplectic Orbit

In order to implement a computer program that can generate the symplectic orbit of given initial conditions for a particular polygon, I have chosen to use Python. An N-sided polygon is represented by a list of vectors (i.e. a `PolyVector`) that designate the vertices of the polygon γ. Initial conditions are provided in the form $(t_0, \bar{u}_0)$, where $t_0 \in [0, N)$ and $\bar{u}_0$ is a vector in $\mathbb{R}^2$. The datum t_0 represents the temporal position along γ where the initial position $x_0 = x(t_0)$ lies. The unit digit of t (i.e., $\lfloor t \rfloor$) represents which edge the point lies on. The fractional part is the linear interpolator of the two endpoints $v_{\lfloor t \rfloor}$ and $v_{\lfloor t \rfloor + 1}$. For corresponding $t \in [0, N)$ and x on edge i, we have the correspondence

$$x(t) = v_{i+1} \cdot t + v_i \cdot (1 - t) \leftrightarrow t(x) = \frac{x - v_i}{v_{i+1} - v_i}, \qquad i = \lfloor t \rfloor.$$

We begin the orbit process by finding t_1: the temporal position of x_1. We say

$$x_1 = \gamma \cap \{s \cdot \hat{u}_0 + x_0 : s \in \mathbb{R}\} \setminus \{x_0\}.$$

Computationally, we define a routine `findIntersection` which can locate the intersection of a line and the polygonal curve. The method iterates over each edge γ_i and calculates the intersection point between the two lines. If the intersection point occurs at a point between the two endpoints (i.e. at a time between i and $i + 1$), then the intersection point is returned. Otherwise, the method continues until finding one. Convexity of the polygonal curve implies that this method behaves well.

Now, given t_0 and t_1, we define $\hat{u}_1 = T_{x_{t_1}} \gamma$, the unit vector parallel to the side on which $x_1 = x(t_1)$ lies, i.e. $\gamma_{\lfloor t_1 \rfloor}$. Then we set

$$x_2 = \gamma \cap \{s \cdot \hat{u}_1 + x_0 : s \in \mathbb{R}\}.$$

Again, this intersection point is calculated with `findIntersection`. Continuing, we define

$$x_n = \gamma \cap \{s \cdot \hat{u}_{n-1} + x_{n-2} : s \in \mathbb{R}\}.$$

Now we must describe the exiting conditions for this symplectic orbit method.

- If there is to exist an $n \in \mathbb{N}$ so that $t_n \approx t_0$, $t_{n+1} \approx t_1$, ..., and $t_{n+Z} \approx t_Z$ for $Z \in \mathbb{N}$, then we conclude that the orbit (x_0, x_1) is periodic of period n. Equality is judged by setting the parameter ϵ that measures proximity: i.e.

$$t \approx t' \iff |t' - t| < \epsilon.$$

  We let Z be large in order to ensure the orbit is truly repeating itself.

- If there is to exist an $n \in \mathbb{N}$ and $k \in \{0, ..., N - 1\}$ so that $t_n \approx_v k$, then we conclude that the orbit has landed at a vertex, making the orbit process undefined beyond this point. We measure proximity to a singularity by $\epsilon_v > 0$, where

$$t \approx_v t' \iff |t' - t| < \epsilon_v.$$

- If initial conditions are such that $T_{x_0}\gamma = T_{x_1}\gamma$, then no next point may be found. So the process is terminated.

- Finally, if no other catches halt the process, we implement an artificial condition that prevents the program from continuing along a non-periodic orbit indefinitely. We define $M \in \mathbb{N}$, so that any orbit having already taken M steps without hitting a singularity nor being reported as periodic is reported as non-periodic up to M steps.
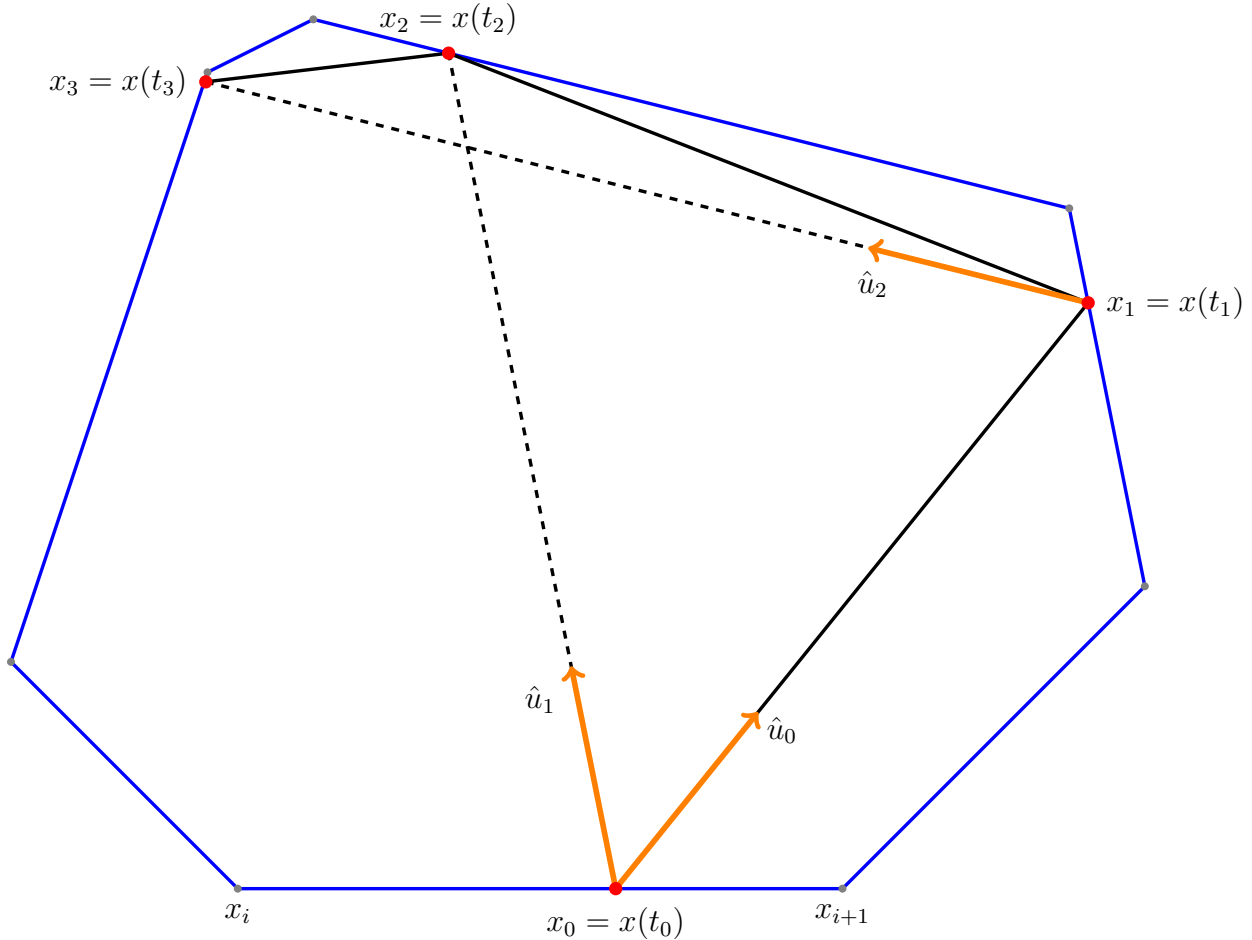

Figure 4.1: An example of the first few steps of calculating the orbit given initial conditions $x_0 = x(t_0)$ and $\hat{u}_0$ on this heptagon. For every $j > 0$, $\hat{u}_j$ is the unit vector based at $x_{j-1} = x(t_{j-1})$ and parallel to the edge of the polygon on which $x_j = x(t_j)$ lies, intersecting the polygonal boundary again at $x_{j+1} = x(t_{j+1})$.

4.2 Sampling Procedure

With such a program, we may conduct a sample of the space of affine quadrilaterals $\mathcal{Q}$ and analyze the behavior of our candidates. Below we will explain the general procedure of sampling this

domain, and then we will review some findings. Recall that $\mathcal{Q}$ is defined as the region satisfying

$$\mathcal{Q} := \{y > 0, y \le x, y > 1 - x\}.$$

Every sample will consist of choosing $S \in \mathbb{N}$ many candidates for the fourth coordinate of the quadrilateral P, where the vertices of the quadrilateral are $\{(0,0), (1,0), P, (0,1)\}$. We define $R > 1/\sqrt{2}$ as the maximum modulus of the fourth coordinate P. For each quadrilateral, we will produce $T \in \mathbb{N}$ many initial conditions $(t_0, \theta_0) \in [0, 4) \times [0, 2\pi)$, where $\hat{u}_0 = (\cos(\theta_0), \sin(\theta_0))$.

- A `Random` sample will select P from a uniform distribution of $\mathcal{Q}$ (up to maximum modulus R).

- A `Rational Angles` sample will specifically consider P so that the internal angles of the resulting quadrilateral are commensurable π. Specifically, a quadrilateral is produced for each positive rational number less than 1, having denominator $1 \le q \le Q$.

- A `Kite` sample will specifically consider P along the line $y = x$, whose corresponding quadrilateral is, in fact, a kite.

4.3 Observed Behaviors

A variety of behaviors can be exhibited from simply the space of affine quadrilaterals under symplectic billiards.

The following Figure 4.2 will compare two orbits along the same quadrilateral that resembles a trapezoid. The first will be periodic and correspond to a periodic orbit along a resembling trapezoid, while the other orbit will be non-periodic up to $M = 1,000$ steps. This example will strongly suggest the possibility for a quadrilateral to possess both periodic and non-periodic orbits, a complex behavior.
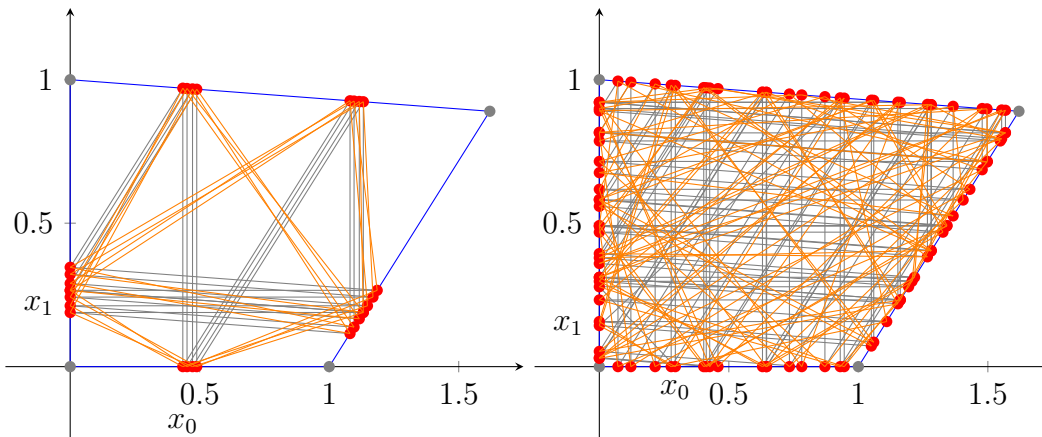

Figure 4.2: Both quadrilaterals are identical: $P = (1.62, 0.89)$, resembling a trapezoid of similar $x_P \approx 1.62$ and $y_P = 1$. The initial condition on the left ($t_0 = 0.5652, \theta_0 = 334°$) produces a 28-periodic orbit. The initial condition on the right ($t_0 = 0.7065, \theta_0 = 334°$) produces a non-periodic orbit up to $M = 1,000$. Only the first 100 steps are displayed in this figure for convenience.

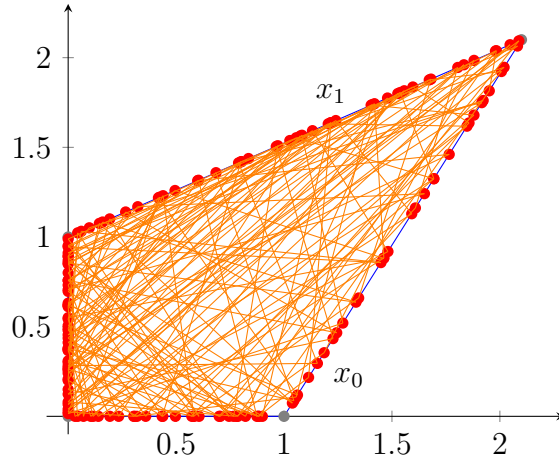The following Figure 4.3 illustrates how non-periodic orbits arise on kites.

Figure 4.3: An example of a kite ($P = (2.1, 2.1)$) without any indication of periodicity up to $M = 1,000$. Initial conditions to create this figure were $t_0 = 1.1034$ and $\theta_0 = 1$.

After tens of thousands of tests, no example of a periodic orbit along a kite has been found. Even kites with integral coordinates exhibited the same behavior. It is reasonable to assume that one could prove a non-periodicity result on this simple shape, but if so, it is not yet obvious why no periodic orbit could exist on a kite.

It is worth noting that this computational method is best at hunting for non-isolated periodic points in phase space. So these results do not speak to isolated periodic orbits.

Next, we sample quadrilaterals with rational angles. We again notice a multitude of behaviors. First, we do find quadrilaterals possessing periodic orbits. Two examples are provided in Figure 4.4.
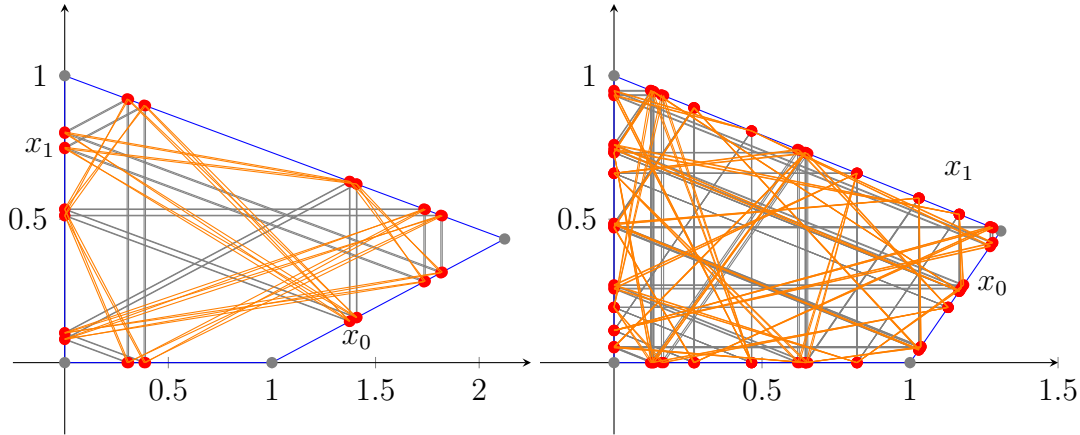

Figure 4.4: Two examples of periodic orbits on a quadrilaterals of rational angles. Left, a quadrilateral made of angles $\pi/2$, $53\pi/60$, $\pi/5$, and $5\pi/12$ (so $P \approx (2.123, 0.431)$), with initial conditions $t_0 = 2.6630$ and $\theta_0 = 175°$. The orbit is 36-periodic. Right, a quadrilateral made of angles $\pi/2$, $11\pi/6$, $7\pi/16$, and $3\pi/8$ (so $P \approx (1.3066, 0.4588)$), with initial conditions $t_0 = 3.4142$ and $\theta_0 = 273°$. The orbit is 132-periodic.

However, there are numerous examples where a quadrilateral of rational angles exhibits non-periodic orbits (up to $M = 1,000$). In fact, none of the combinations of rational angles tested produced quadrilaterals which had no non-periodic orbits (in other words, every tested quadrilateral possessed a non-periodic orbit). In fact, taking the second example from Figure 4.4, any minute alteration made to the initial conditions made a non-periodic orbit, showing how relatively isolated that example is on that quadrilateral. Some shapes were more likely to produce periodic orbits than others. We will present those sets of angles by two internal angles: those adjacent to the right angle, and the value of the third angle (opposite the right angle) will be implied from the rest. Those sets of angles for which orbits were often periodic included:

$$(\alpha, \beta) \in \left\{ \left(\frac{7\pi}{12}, \frac{35\pi}{48} \right), \left(\frac{7\pi}{12}, \frac{7\pi}{12} \right) \right\}.$$

Obviously, not many exhibited this property. Some of the sets of angles that provided some of the worst conditions for producing periodic orbits included:

$$(\alpha, \beta) \in \left\{ \left(\frac{5\pi}{12}, \frac{29\pi}{36} \right), \left(\frac{5\pi}{12}, \frac{9\pi}{16} \right), \left(\frac{5\pi}{12}, \frac{23\pi}{30} \right), \left(\frac{7\pi}{12}, \frac{5\pi}{8} \right), \left(\frac{7\pi}{12}, \frac{\pi}{2} \right), \left(\frac{3\pi}{8}, \frac{11\pi}{16} \right) \right\}.$$

There is no obvious way to discern between these two sets yet, but regardless, we note that each quadrilateral of rational slope seems to provide both types of periodicity.

This property extends to the full space of affine quadrilaterals. Periodicity appears to be a special property for an initial condition on a generic quadrilateral. However, this property appears often enough to suggest that it does not just occur on a set of measure zero. Its abundance seems to exist around 18% in random conditions, but the ability to verify these results for larger maximum modulus R of P quickly dissolves, so this will have to be verified in another effort.

Bibliography

[1] P. Albers and S. Tabachnikov. Introducing symplectic billiards, last accessed on 04/07/2019 at https://www.math.psu.edu/tabachni/prints/notes5.pdf.

[2] F. L. Owen Bryer and D. L. Smeltzer. *Methods for Euclidean Geometry*. Classroom Resource Materials. Mathematical Association of America, 2010.

Academic Vita — Raymond Friend

April 7, 2019

Mathematics and Physics

Education

- **Schreyer Honors College** — University Park, PA, USA
  The Pennsylvania State University — August 2015 - May 2019
    - BS in Mathematics, Graduate option.
    - BS in Physics, General option.

- **MASS Program at Penn State** — University Park, PA, USA
  Mathematical Advanced Study Semester — Fall 2016, Fall 2017
    - Presented four projects over these two semesters. Best Projects in Algebra 2016 & 2017.
    - Combined knowledge from curriculum with my own reading and calculations.
    - Collaborated with instructors and learning assistants frequently.

Research Experience

- **Auburn University REU in Mathematics** — Auburn, AL, USA
  Ramsay Theory and Abstract Algebra — June-July 2018
    - Generalized Achievement Sets of Sequences to Groups, also solving an open question.
    - Constructed counterexamples to existing conjectures for simple, oriented graphs.
    - Presented my findings at the Clemson University REU Conference.

- **Wealth Sharing Problem** — University Park, PA, USA
  With Dr. Misha Guysinsky — January-August 2017
    - Developed methods for showing how a particular trading of wealth produces a Benford distribution.
    - Examined current literature for relevant results.

- **HAWC Observatory** — University Park, PA
  Research Assistant — September 2015-September 2016
    - Developed a neural network that could reliably distinguish between gamma and cosmic rays for the purpose of refining data.
    - Improved models for air showers used in recreating shape of incoming cones of particles.

Leadership Experience

- **Math Club** — University Park, PA, USA
  Vice President & Treasurer — April 2016-April 2018
    - Established records of past and future finances.
    - Networked with with PSU faculty to coordinate talks.
    - Created material for competitions and lectures to the club.